VERTICAL PROFILE FOR CO_2 AND PARTICLE DISTRIBUTION FROM VENUS' MASS SPECTRA. R. Mogul[1], S. L. Limaye[2], M. Way[3], [1]Cal Poly Pomona (rmogul@cpp.edu), [2]Univ. of Wisconsin, Madison, [3]NASA Goddard Institute for Space Studies.

Introduction: We present a new analysis and interpretation of mass spectral profiles obtained by the Pioneer Venus (PV) Large Probe Neutral Mass Spectrometer (LNMS) [1, 2], which descended into Venus' atmosphere on December 9, 1978, and collected data across the altitudes of 64-0.9 km. To analyze the data, we constructed an analytical model and data-fitting routine that accounts for changes in the performance of the spectrometer at each altitude, and provides estimates of atmospheric abundances in units of density (kg/m^3). Our approach represents a significant advance in interpretation of the archived mass spectra and maximizes output by retaining the resolving power of the LNMS and minimizes biases that would arise from data binning procedures due to the non-uniformly distributed mass points obtained by the LNMS (between *m/z* 1-208).

Methods: Our data-fitting routine along the altitude profile yields quantitative measures of peak width (and variance), accounts for shifts in the mass scale, and includes relevant isobaric species. Data were judiciously normalized to account for the valve openings (~64 km) and closure (~47 km) and the related changes in atmospheric intake rates. Lastly, CO_2 counts were converted to density (kg/m^3) using standard curves constructed from published control data.

Results & Discussion: *Statistical Treatments*. Minimum standard deviations for the ion counts were obtained by analysis of mass positions in the pre-sampling data for CH_4^+, CH_3^+, $^{40}Ar^+$, and $^{136}Xe^+$ (which were fitted as described in Mogul (2021)), and $^{13}CH_4^+$, CH_2^+, and C^+ (which were represented by one mass point). Errors were propagated throughout the calculations.

Performance of the LNMS. We tracked several species across the altitude profile and pre-sampling data to obtain insights into the operations of the mass analyzer. As summarized in **Fig. 1**, we calculated peak widths and centroids for CH_3^+, $^{40}Ar^+$, and $^{136}Xe^+$, which were treated as internal standards. Across the profiles, in **Fig. 2**, minimal variances are observed for peak widths (full width half maximum, FWHM) and peak centroids ($\Delta(m/z)$). These total trends reveal (1) a linear correlation (R^2 >0.99) between FWHM and *m/z* at each altitude, consistent with the results of Mogul (2021), and (2) that the LNMS exhibited no anomalous operations throughout the descent, especially between (A) 50-25 km, where the inlets to the LNMS were clogged by aerosol particles, and (B) at <20 km, where atmospheric pressures and temperatures were substantially higher.

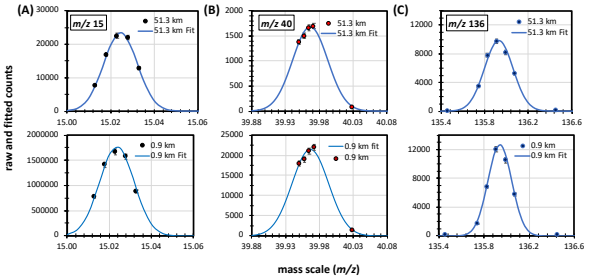

Figure 1. Example Gauss peak fits at 51.3 and 0.9 km for the internal standards of (A) CH_3^+ (*m/z* 15), (B) $^{40}Ar^+$ (*m/z* 40), and (C) $^{136}Xe^+$ (*m/z* 136); mass scale is represented as *m/z*, y-axis is scaled for clarity due to changing abundances (CH_3^+ & $^{40}Ar^+$), and error bars represent the minimum standard deviation.

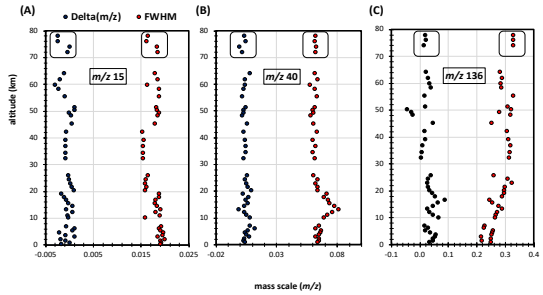

Figure 2. Altitude profiles (64.2-0.9 km) showing changes in peak widths (FWHM; red circles) and peak centers ($\Delta(m/z)$ = calculated mass – exact mass; blue circles) for (A) CH_3^+ (*m/z* 15), (B) $^{40}Ar^+$ (*m/z* 40), and (C) $^{136}Xe^+$ (*m/z* 136), inclusive of the pre-sampling mass sweeps, which are nominally listed between 78-72 km for clarity (rounded boxes).

Ionization and Fragmentation of CO_2. In **Figs. 3A-B** are profiles for the CO_2 ionization and fragmentation products of $CO^{18}O^+$, $^{13}CO_2^+$, $C^{18}O^+$, $^{13}CO^+$, $^{13}CO_2^{++}$, and CO_2^{++}. Abundances are expressed relative to CO_2^+; averages and standard deviations were calculated across the clouds (58.8-51.3 km) and lower atmosphere (24.4-0.9 km). For ionized CO_2 and isotopologues, values across the profile for $CO^{18}O^+$ (0.44 ± 0.03%), $^{13}CO_2^+$ (1.3 ± 0.1%), $^{13}CO_2^{++}$ (0.033 ± 0.002%), and CO_2^{++} (2.6 ± 0.1%) exhibited minimal variances and are similar – though slightly higher – than NIST values for $CO^{18}O^+$ (~0.3%), $^{13}CO_2^+$ (~1.1%), and CO_2^{++} (~1.8%). Values for other fragments, including isobars for all species, will be discussed.

Isotope Ratios. Tracking of $CO^{18}O^+$, $^{13}CO_2^+$, $^{13}CO_2^{++}$, and $C^{18}O^+$ along the profile, excluding the main clog, yields averaged isotope ratios of 0.22 ± 0.02% for

$^{18}O/^{16}O$, and aggregated values of 1.30 ± 0.10% for $^{13}C/^{12}C$ from $^{13}CO_2^+/CO_2^+$ and $^{13}CO_2^{++}/CO_2^{++}$.

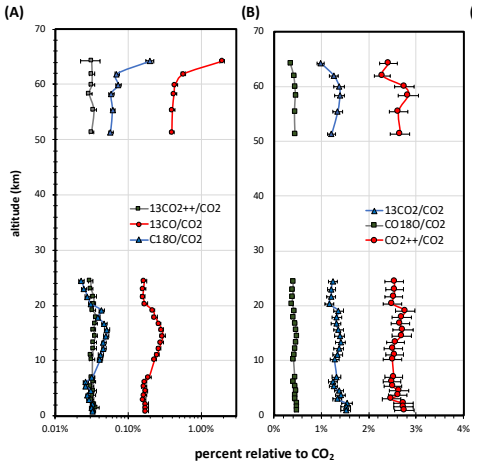

Figure 3. Altitude profiles (64.2-0.9 km) for ionized and fragmented products of CO_2 inclusive of $CO^{18}O^+$, $^{13}CO_2^+$, $C^{18}O^+$, $^{13}CO^+$, $^{13}CO_2^{++}$, and CO_2^{++}, which are organized as (A) $^{13}CO_2^{++}$, $C^{18}O^+$, and $^{13}CO^+$ (log scale), and (B) $CO^{18}O^+$, $^{13}CO_2^+$, and CO_2^{++} (linear scale); error bars represent the propagated error.

Profiles for CO_2 and Atmospheric Density. In **Fig. 4,** we provide the CO_2 altitude profile (red circles) expressed as percent of the atmospheric densities, which were calculated using data from Seiff (1985). Measured densities for CO_2 fluctuated greatly over the descent as duly observed between 50-25 km (large blue block arrow in **Fig. 4**) where the LNMS inlets were clogged. However, when intake rates were optimal, our analyses yield a CO_2 density at 51.3 km (1.36 ± 0.27 kg/m^3) that is 98 ± 19% of the atmospheric density (1.38 kg/m^3), while densities between 23.0-17.9 km (14.9-21.1 kg/m^3) are ~91 ± 4% of the respective atmospheric values (16.7-23.3 kg/m^3). From ~17 km towards the surface, CO_2 densities retained high percentages but temporarily deviated from the atmospheric profile, as labeled in **Fig. 4** (green block arrows), to yield 'dips' between 16.7-13.3 km (≤30% decreases) and 13.2-7.0 km (≤25% decreases).

These observations are consistent with the LNMS experiencing partial and rapidly-clearing clogs in the lower atmosphere (<17 km) due to particulate and/or aerosol species. In support, in **Fig. 4** the CO_2 profile is compared to the scattering extinction coefficients measured by Venera 13 and 14 [4] and the PV Large Probe [5]. In summary, *increases* in particle densities (or cross sections) between ~50-46 and ~17-2 km match the altitude ranges where CO_2 densities *decrease* between 50-25 and 16.7-5.3 km. Interpretations of the mass data within this context will be presented.

Conclusions: The LNMS measurements represent the most robust detection of CO_2 across Venus' atmosphere to date. The $^{18}O/^{16}O$ and $^{13}C/^{12}C$ ratios are similar to the Earth abundances, and the listed fragmentation yields are similar to NIST values. Densities for CO_2 increase towards the surface, which is suggestive of surface outgassing [6]. Lastly, we show that atmospheric intake into the LNMS was partly obstructed by particles and/or aerosols at <17 km, which impacts interpretation of data from the lower atmosphere. Such considerations are likely critical for future mass spectral investigations. Thus, our current and forthcoming results bolster those presented in Mogul (2021) and demonstrate the benefits of thorough re-analyses of the LNMS data for Venus science.

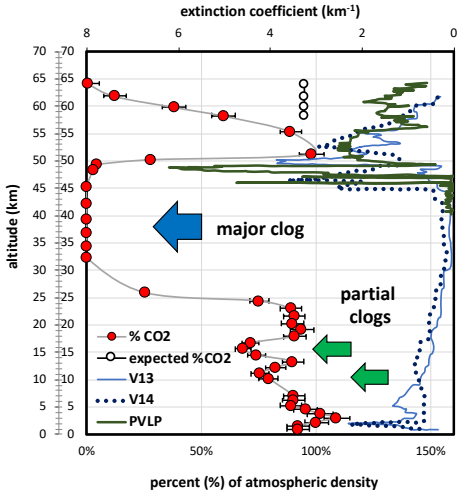

Figure 4. Altitude profiles for %CO_2 (relative to atmospheric densities; red circles) and the volumetric scattering coefficients (upper x-axis, reversed scale) measured by Venera 13 (solid blue line), Venera 14 (dotted black line), and the Pioneer Venus (PV) Large Probe (solid thick green line); block arrows represent areas of partial blockage of the inlets, expected CO_2 values are provided ≥58 km (circles), and error bars represent the propagated error.

Acknowledgments: RM was supported by a NASA NExSS grant (80NSSC21K1176). MJW was supported by NASA's NExSS and GSFC-SEEC. The LNMS data are online at the NSSDCA (PSPA-00649).

References:

[1] Hoffman, J.H., et al. (1980) J. Geophys. Res. Space Phys., *85*, 7882-7890. [2] Mogul, R., et al. (2021) Geophys. Res. Letters, *48*, e2020GL091327. [3] Seiff, A., et al. (1985) Adv. Space Res., *5*, 3-58. [4] Grieger, B., et al. (2004) Proc. Int. Workskhop "Planetary Probe Atmospheric Entry and Descent Trajectory Analysis and Science", *544*, 63-70. [5] Ragent, B., et al. (1985) Adv. Space Res., *5*, 85-115. [6] Cordier, D., et al. (2019) The Astrophys. J., *880*, 82.